Eur Phys J C **40**, s02, 1–13 (2005)
Digital Object Identifier (DOI) 10.1140/epjcd/s2005-02-001-5

EPJ C direct
electronic only

Scientific Note

The efficiency of the CMS Level-1 Trigger for supersymmetric events

L. Boldizsár[1], J. Erö[2], M. Fierro[2], P. Hidas[1], A. Jeitler[2], N. Neumeister[2], P. Porth[2], H. Rohringer[2], L. Rurua[2], H. Sakulin[2], A. Taurok[2], C.-E. Wulz[2,a]

[1] KFKI Research Institute for Particle and Nuclear Physics, Konkoly T. M. út. 29-33, 1121 Budapest, Hungary
[2] Institute for High Energy Physics of the Austrian Academy of Sciences, Nikolsdorfergasse 18, 1050 Vienna, Austria

Received: 4 May 2004 / Revised version: 17 January 2005 /
Published online: 14 March 2005 –

Abstract. The performance of the CMS Level-1 Trigger for supersymmetric events at an LHC luminosity of 2×10^{33} cm^{-2}s^{-1} is reviewed. Energy and momentum trigger thresholds have been chosen to yield a maximum Level-1 output rate of 50 kHz, within a safety factor of three. The Level-1 trigger efficiencies for the majority of the channels studied are found to be greater than 90%, which provides a good basis for the High-Level Trigger, where more stringent conditions are applied. Reasons for occasional lower efficiencies are given.

1 Introduction

The Large Hadron Collider (LHC) is presently under construction at CERN, the European Organization for Nuclear Research in Geneva. The initial luminosity for proton-proton collisions at 14 TeV centre-of-mass energy is expected to be $2 \times 10^{33}\,\mathrm{cm}^{-2}\,\mathrm{s}^{-1}$. At this luminosity, also referred to as low luminosity, an average of 3.5 proton-proton interactions will occur every 25 ns, corresponding to a bunch crossing frequency of 40 MHz. In practice the number of filled bunches in the LHC ring is 2808 out of a total of 3564. The average bunch crossing rate is therefore 31.5 MHz, leading to an interaction rate of more than 100 MHz. Because it is impossible to store and process the large amount of data associated with the resulting high number of events, a drastic rate reduction has to be achieved. This task is performed by the trigger system, which is the start of the physics event selection process.

In CMS (Compact Muon Solenoid), one of two multi-purpose experiments at the LHC, the input rate is reduced in two steps called Level-1 (L1) Trigger [1] and High-Level Trigger (HLT) [2] respectively. A decision to retain an event for further consideration has to be made by the L1 Trigger for each bunch crossing. This decision is based on an event's suitability for inclusion in one of the various data streams to be used for analysis. The data sets to be recorded are determined by CMS physics priorities. They include data sets triggered with single leptons and dileptons, mainly for Higgs boson and other discovery searches as well as for beauty and heavy ion physics. Data sets triggered with leptons plus jets are important for supersymmetry (SUSY) and top physics, and inclusive electron data sets are useful for calorimeter calibration. Other samples are necessary for measuring event selection efficiencies and studying backgrounds. The trigger has to select all events in real time.

The L1 Trigger has to take the decision to accept or reject an event for each bunch crossing with negligible deadtime. The crossing interval of 25 ns is too short to process the complete trigger information. A pipelined system that stores the data during a latency time of 3.2 μs has therefore been conceived. The rate reduction capability is designed to be at least a factor of 10^6 for the combined L1 and HLT, as the highest rate that can be archived by the on-line computer farm is of the order of 100 Hz. The maximum bandwidth allocated to the L1 Trigger is 100 kHz, in accordance with the input capacity limit of the HLT processor farm. At the startup of LHC, it will, however, be reduced to 50 kHz for operational reasons.

In this paper, the trigger efficiencies for SUSY events are determined at the end of the Level-1 chain, i.e. at the output of the Global Trigger. The CMS Global Trigger takes the decision to accept or reject an event at L1. It is based on input from the Global Calorimeter and Global Muon Triggers, which process information from the Regional Triggers of the calorimeters and the muon system. The CMS Muon Trigger is special in the sense that both the precision tracking chambers, made up of drift-tubes in the barrel and cathode strip chambers in the endcaps, and dedicated resistive plate trigger chambers take part in the

[a] e-mail: Claudia.Wulz@cern.ch

trigger. The Local Triggers for calorimetry and muons, at the bottom end of the trigger chain, are based on energy deposits in calorimeter trigger towers and track segments in muon chambers, respectively.

In the following chapters, the CMS Level-1 Trigger (Sect. 2), the simulated physics channels (Sect. 3) and the detector and trigger simulation (Sect. 4) are described, followed by a definition of the applied trigger scenario (Sect. 5). Finally, the results on trigger efficiencies obtained with the trigger menu used are presented and discussed in Sect. 6.

2 The Level-1 Trigger

The Level-1 Trigger operates on the basis of trigger objects delivered by the calorimeter and muon trigger systems. These objects are candidate electrons or photons, muons, jets, hadronic τ decays (called "τ jets" in the following) as well as total and missing transverse energies and jet multiplicities. Neither the silicon inner tracker nor the pixel vertex detector take part in the Level-1 Trigger. Objects representing particles are characterized by their location, their transverse momentum or energy and quality. The latter reflects the level of confidence attributed to the Level-1 parameter measurements, based on detailed knowledge of the trigger detectors and electronics and on the amount of information available. Objects are sorted by rank, which is a function of momentum or energy, and, to a lesser extent, of quality.

The calorimeter consists of a homogeneous electromagnetic part made of lead-tungstate crystals and a hadron part made of brass and scintillator samples in the barrel and endcap regions and quartz fibres embedded in an absorber matrix in the forward region. The first step of the Calorimeter Trigger consists in summing the energies measured in cells within electromagnetic and hadron trigger towers. In the region up to $|\eta| \approx 2$ each trigger tower has a pseudorapidity-azimuth (η-ϕ) coverage of 0.087×0.087 rad. Beyond that boundary the towers are larger. The Regional Calorimeter Trigger [1,3] then determines candidate electrons, jets, τ jets and transverse energy sums. The candidates found in a region of $\Delta\eta \times \Delta\phi = 3.0 \times 0.7$ rad, that is one trigger crate in hardware, are then ranked according to transverse energy (E_T) and quality. The four highest-rank candidates in each region are transmitted to the Global Calorimeter Trigger [4], which in turn determines the four highest-rank calorimeter trigger objects across the whole detector.

Electrons and photons are indistinguishable at the level of the L1 Trigger in the absence of tracker information. The electron/photon trigger algorithm is depicted in Fig. 1. It is applied across the entire (η, ϕ) plane and starts by determining the tower with the largest energy deposit. The energy of the tower with the next-highest deposit in one of the four broad side neighbours is then added. Isolated and non-isolated electrons/photons are determined by the trigger. A non-isolated electron/photon requires passing of two shower profile vetoes. The first one is based on a fine-grain crystal energy profile reflecting the

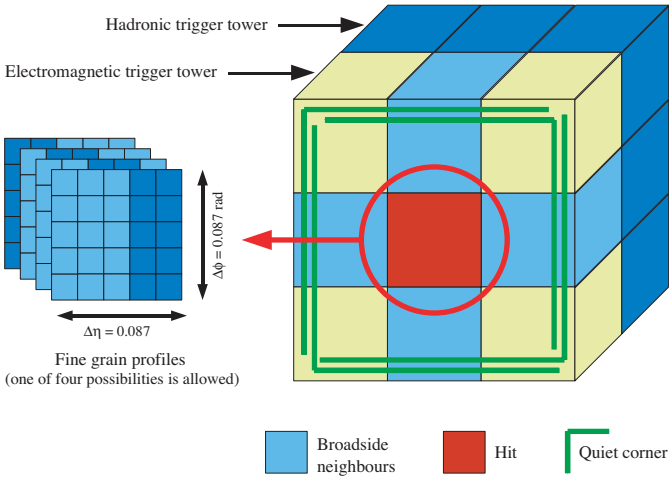

Fig. 1. Electron/photon trigger algorithm

lateral extension of a shower. The fine-grain bit is set if the shower is contained in a matrix of 2×5 crystals. The second one is based on the ratio of the deposited energies in the hadron and in the electromagnetic sections. A typical maximal value of 5% is allowed for that ratio. An isolated electron/photon candidate has to pass the previous vetoes for all eight neighbouring towers. In addition, at least one quiet corner made of four groups of five towers surrounding the hit tower is required.

Jets are found by a technique using a sliding window of 3×3 calorimeter regions corresponding to 12×12 trigger towers in the barrel and endcaps and covering a region of $\Delta\eta \times \Delta\phi = 1.04 \times 1.04$ rad. In the forward hadron calorimeter 3×3 trigger towers of larger size than the central towers are grouped together. The window is shifted by one region at a time. The transverse energy of the region made up by the 4×4 central trigger towers is required to be higher than the eight neighbour region values. It is also required to be larger than 1 GeV to suppress spurious contributions.

The τ jets from one- and three-prong τ decays are required to have a transverse energy distribution narrower than ordinary quark/gluon jets. A jet is called a τ jet if none of the nine calorimeter trigger regions has a τ-veto bit on. A veto bit is set unless the pattern of active towers corresponds to at most 2×2 contiguous trigger towers within a 4×4 tower region.

In addition to electrons and jets, the Regional Calorimeter Trigger also delivers transverse energy sums and jet multiplicities to the Global Calorimeter Trigger. The latter determines the total transverse energy, the magnitude and direction of the missing transverse energy computed from the tower energy measurements in the two coordinates transverse to the beam within $|\eta| < 5$, and twelve jet counts for different energy thresholds and optionally also different η regions. The jet counts were not used in this study, but may be useful to trigger on events with a large number of jets, such as gluino or squark decays. The Global Calorimeter Trigger also delivers H_T, the scalar transverse energy sum of all jets above a pro-

grammable threshold set to 10 GeV in this study. This quantity is less sensitive to noise and pileup than the total transverse energy and is, just like the jet counts, particularly useful if events have many but relatively low energy jets. Such events may actually fail the jet triggers that have to use high thresholds to achieve an acceptable trigger rate.

All three muon subsystems take part in the trigger and can deliver information on transverse momentum (p_T) and location of muon candidates. The tracking chambers in the barrel and in the forward regions are equipped with electronics suitable for triggering. Precise timing information is delivered both by the drift-tube (DT) and cathode strip chambers (CSC). The resistive plate chambers (RPC) mounted on the tracking chambers are dedicated trigger chambers.

The barrel DT chambers have a special Bunch and Track Identifier logic [5] to find track segments from coincidences of aligned hits in four layers of one drift-tube superlayer. All DT chambers have two superlayers to measure azimuth. The segments from these two layers are combined by a track correlator, which works on the basis of the measured angular coordinates. The chambers in the three innermost muon stations have a third superlayer to determine pseudorapidity, with wires orthogonal to those of the two ϕ-superlayers. The fourth outermost muon station has only two ϕ-superlayers.

The trigger electronics of the endcap CSC chambers forms track segments called Local Charged Tracks (LCT) from the cathode strip measurements [6]. These are combined with information from the anode wires for bunch crossing identification. The highest-p_T DT and CSC track segments are sent to the respective regional triggers called Track Finders [7,8]. These Track Finders form muon candidates out of the track segments using extrapolation and pattern matching methods. The RPC's deliver hit patterns. If a pattern matches a predicted one, a muon candidate is established and a p_T value is assigned to it [9].

The trigger information from three different muon subsystems is merged by the Global Muon Trigger [10]. It sorts the DT, CSC and RPC candidates and tries to match them. It achieves an increased efficiency with respect to the three separate muon systems, whilst reducing trigger rates and the occurrence of fake muons. The Global Muon Trigger also correlates muon candidates with regions in the calorimeter in order to confirm minimal ionization and to apply isolation criteria.

The Global Trigger [11] at the top of the L1 Trigger chain issues the Level-1 accept/reject decision. It receives input from both the calorimeters and the muon system. The best four objects of each of the following categories, sorted by transverse energy or momentum and quality, are delivered by the Global Calorimeter and the Global Muon Trigger: isolated and non-isolated electrons or photons in a pseudorapidity range of $|\eta| < 2.5$, central jets in $|\eta| \leq 3$, forward jets in $3 < |\eta| < 5$, τ jets in the central region up to $|\eta| < 2.5$ and muons within $|\eta| \leq 2.1$ at the startup of LHC (later the coverage is foreseen to be enlarged to $|\eta| \leq 2.4$). The remaining trigger objects are the total (ΣE_T) and missing transverse energies ($\not\!\!E_T$), the transverse energy sum of all jets above a programmable threshold (H_T) and the twelve jet multiplicities. A maximum number of 128 physics trigger algorithms running in parallel is possible. An algorithm is a logical combination of objects fulfilling energy, momentum or multiplicity threshold conditions. Topological requirements and veto conditions can also be applied. The algorithm settings are largely programmable.

3 Physics channels and event generation

Supersymmetry is one of the primary search topics at the LHC. In this study, supersymmetric production processes that require in general multi-object triggers as opposed to simple conditions like single leptons or jets have been chosen. Specifically, slepton ($\tilde{\ell}\tilde{\ell} \to \ell^+\ell^-\tilde{\chi}_1^0\tilde{\chi}_1^0$), chargino/neutralino ($\tilde{\chi}_1^\pm\tilde{\chi}_2^0 \to 3\ell\tilde{\chi}_1^0\tilde{\chi}_1^0$) and gluino/squark ($\tilde{\mathrm{g}}/\tilde{\mathrm{q}}$) production were studied. The Drell-Yan produced sleptons and charginos/neutralinos lead to final states with multileptons and missing transverse energy, but no jets. For gluino/squark events, one or more jets can be required in addition by the trigger. WW production has also been included: it is a benchmark process for triggering, since many new particles are predicted to decay into intermediate vector bosons.

A consensus was reached [12,13] to define a list of SUSY models as benchmarks to be investigated in future collider studies. Various scenarios, so-called "Snowmass Points and Slopes" (SPS), were proposed in terms of a few parameters describing "typical" to "extreme" R-parity conserving supersymmetry breaking mechanisms of mSUGRA (minimal supergravity), GMSB (gauge-mediated SUSY breaking) and AMSB (anomaly-mediated SUSY breaking). All benchmark points respect current experimental constraints. By the time LHC starts, a significant integrated luminosity is supposed to be collected at the Tevatron collider. The starting point for LHC is assumed to be the maximal sparticle mass reach for Run II as defined in [14].

Channels with parameters according to selected Snowmass Points and Slopes and, in order to be compatible with HLT studies that focus on probing points at the upper mass reach of Tevatron Run II, general mSUGRA signals [15] were provided by the CMS Physics Reconstruction and Selection Group. The parameters necessary to describe the selected points are $\tan\beta, m_0, m_{1/2}$, the sign of μ and A_0, where $\tan\beta$ is the ratio of the vacuum expectation values of the two Higgs doublets, m_0 and $m_{1/2}$ are the universal scalar mass and universal gaugino mass at the GUT scale of approximately 2×10^{16} GeV/c^2, μ is the Higgsino mass mixing parameter, and A_0 is the universal trilinear coupling. The list of chosen signals is given in the following.

Channel A (smuons at SPS 1a):
$m_0 = 100$ GeV/c^2, $m_{1/2} = 250$ GeV/c^2, $\mu > 0$,
$\tan\beta = 10$, $A_0 = -100$ GeV.
Production: $\tilde{\mu}_L\tilde{\mu}_L$ with $\tilde{\mu}_L^\pm \to \mu^\pm\tilde{\chi}_1^0$

Sparticle mass spectrum:
$m_{\tilde{e}_L,\tilde{\mu}_L} = 211$ GeV/c^2, $m_{\tilde{\nu}_L} = 196$ GeV/c^2,
$m_{\tilde{e}_R,\tilde{\mu}_R} = 146$ GeV/c^2, $m_{\tilde{\tau}_1} = 146$ GeV/c^2,
$m_{\tilde{g}} = 562$ GeV/c^2, $m_{\tilde{t}_1} = 289$ GeV/c^2,
$m_{\tilde{u}_L} = 501$ GeV/c^2, $m_{\tilde{b}_1} = 438$ GeV/c^2,
$m_{\tilde{\chi}_1^0} = 100$ GeV/c^2, $m_{\tilde{\chi}_2^0} = 189$ GeV/c^2,
$m_{\tilde{\chi}_1^\pm} = 188$ GeV/c^2, $m_{\tilde{\chi}_2^\pm} = 398$ GeV/c^2.

Channel B (charginos/neutralinos at SPS 1a):
$m_0 = 100$ GeV/c^2, $m_{1/2} = 250$ GeV/c^2, $\mu > 0$,
$\tan\beta = 10$, $A_0 = -100$ GeV.
Production:
$\tilde{\chi}_2^0\tilde{\chi}_1^\pm \to (\tilde{\tau}_1^\pm\tau^\mp)(\tilde{\tau}_1^\pm\nu_\tau) \to (\tau^+\tau^-\tilde{\chi}_1^0)(\tau^\pm\tilde{\chi}_1^0\nu_\tau) \to$
$\to 3l2\tilde{\chi}_1^0 4\nu_\tau 3\nu_l$ where l = e or μ.
Sparticle mass spectrum: as for channel A.

Channel C (gluinos/squarks at SPS 1a):
$m_0 = 100$ GeV/c^2, $m_{1/2} = 250$ GeV/c^2, $\mu > 0$,
$\tan\beta = 10$, $A_0 = -100$ GeV.
Production: $\tilde{g}\tilde{g}, \tilde{g}\tilde{q}, \tilde{q}\tilde{q}$
Sparticle mass spectrum: as for channel A.

Channel D (gluinos/squarks at SPS 2):
$m_0 = 1450$ GeV/c^2, $m_{1/2} = 300$ GeV/c^2, $\mu > 0$,
$\tan\beta = 10$, $A_0 = 0$ GeV.
Production: $\tilde{g}\tilde{g}, \tilde{g}\tilde{q}, \tilde{q}\tilde{q}$
Sparticle mass spectrum:
$m_{\tilde{\ell}_L} = 1456$ GeV/c^2, $m_{\tilde{\ell}_R} = 1452$ GeV/c^2,
$m_{\tilde{\tau}_1} = 1439$ GeV/c^2, $m_{\tilde{q}} = 784$ GeV/c^2,
$m_{\tilde{t}_1} = 1003$ GeV/c^2, $m_{\tilde{u}_L} = 1532$ GeV/c^2,
$m_{\tilde{b}_1} = 1297$ GeV/c^2,
$m_{\tilde{\chi}_1^0} = 122$ GeV/c^2, $m_{\tilde{\chi}_2^0} = 239$ GeV/c^2,
$m_{\tilde{\chi}_1^\pm} = 239$ GeV/c^2, $m_{\tilde{\chi}_2^\pm} = 677$ GeV/c^2.

Channel E (mSUGRA4):
$m_0 = 20$ GeV/c^2, $m_{1/2} = 190$ GeV/c^2, $\mu > 0$,
$\tan\beta = 10$, $A_0 = 0$ GeV.
Production: all processes allowed within the mSUGRA model

Sparticle mass spectrum:
$m_{\rm h} = 110$ GeV/c^2, $m_{\tilde{g}} = 466$ GeV/c^2,
$m_{\tilde{u}_L} = 410$ GeV/c^2,
$m_{\tilde{\chi}_1^0} = 70$ GeV/c^2, $m_{\tilde{\chi}_2^0} = 126$ GeV/c^2,
$m_{\tilde{\chi}_1^\pm} = 125$ GeV/c^2, $m_{\tilde{\chi}_2^\pm} = 296$ GeV/c^2.

Channel F (mSUGRA5):
$m_0 = 150$ GeV/c^2, $m_{1/2} = 180$ GeV/c^2, $\mu > 0$,
$\tan\beta = 10$, $A_0 = 0$ GeV.
Production: all processes allowed within the mSUGRA model
Sparticle mass spectrum:
$m_{\rm h} = 110$ GeV/c^2, $m_{\tilde{g}} = 447$ GeV/c^2,
$m_{\tilde{u}_L} = 415$ GeV/c^2,
$m_{\tilde{\chi}_1^0} = 66$ GeV/c^2, $m_{\tilde{\chi}_2^0} = 119$ GeV/c^2,
$m_{\tilde{\chi}_1^\pm} = 117$ GeV/c^2, $m_{\tilde{\chi}_2^\pm} = 285$ GeV/c^2.

Channel G (mSUGRA6):
$m_0 = 300$ GeV/c^2, $m_{1/2} = 130$ GeV/c^2, $\mu > 0$,
$\tan\beta = 10$, $A_0 = 0$ GeV.
Production: all processes allowed within the mSUGRA model
Sparticle mass spectrum:
$m_{\rm h} = 106$ GeV/c^2, $m_{\tilde{g}} = 349$ GeV/c^2,
$m_{\tilde{u}_L} = 406$ GeV/c^2,
$m_{\tilde{\chi}_1^0} = 45$ GeV/c^2, $m_{\tilde{\chi}_2^0} = 80$ GeV/c^2,
$m_{\tilde{\chi}_1^\pm} = 77$ GeV/c^2, $m_{\tilde{\chi}_2^\pm} = 233$ GeV/c^2.

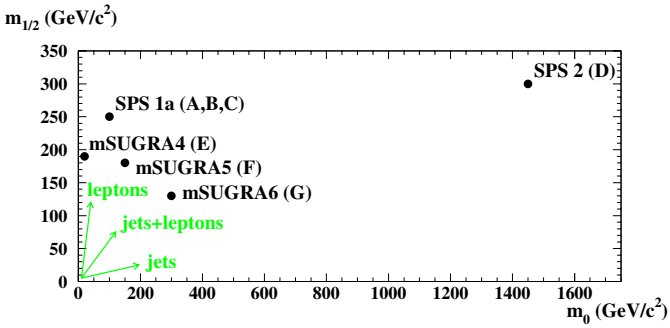

Fig. 2. The position of the generated samples on the (m_0 – $m_{1/2}$) plane

Channel H (WW):
Production: W^+W^- with $W \to \mu\nu_\mu$

The positions of the points chosen on the ($m_0 - m_{1/2}$) plane are shown in Fig. 2. The gluino/squark production channels are expected to yield substantial missing transverse energy. In the case of SPS 1a (channels A, B and C) mostly leptons are expected, whilst for SPS 2 (channel D) jets dominate. The mSUGRA4 channel (E) is τ-enriched and has several leptons. The characteristics of the mSUGRA5 channel (F) are jets and leptons. The mSUGRA6 channel (G) has even more jets, but less missing transverse energy due to balanced contributions from several neutralinos and neutrinos. This fact is illustrated in Fig. 3, which shows the number of jets (central, forward and τ jets) and the missing transverse energy distributions of the mSUGRA samples as measured by the Level-1 Trigger.

All physics channels were simulated with Monte Carlo event generators. The program PYTHIA 6.158 [16,17] was used to simulate channels A, B, C, D and H. Channels E, F and G were generated with ISAJET 7.51 [18]. The proton parton distribution functions CTEQ 5L [19] were chosen for both Monte Carlo programs. For each SUSY sample (channels A to G) 1000 events were generated. 2000 events were produced for the WW sample (channel H). The cross sections of channels A to H and the number of events expected after one LHC year corresponding to an integrated luminosity of 20 fb^{-1} are summarized in Table 1.

To reproduce the real conditions of data taking, with on average 3.5 proton-proton interactions (in-time pileup) taking place per bunch crossing in a 25 ns time window, minimum bias events had to be added to each signal event. They were generated with PYTHIA 6.158.

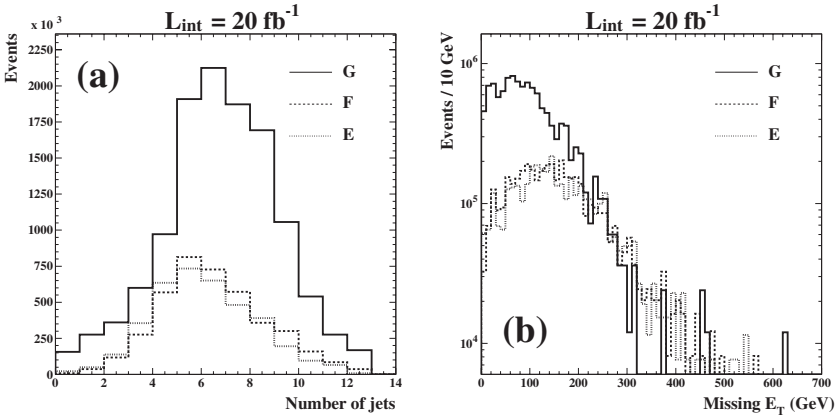

Fig. 3. Distributions of **a** the number of jets and **b** the missing transverse energy for the mSUGRA channels E, F and G

Table 1. Cross sections and expected number of events of channels A to H for one year of LHC running (20 fb^{-1})

Channel	Sample	Cross section [pb]	Number of events per LHC year
A	Smuons at SPS 1a	0.110	$2.20 * 10^3$
B	Charginos/neutralinos at SPS 1a	0.267	$5.34 * 10^3$
C	Gluinos/squarks at SPS 1a	2360	$4.72 * 10^7$
D	Gluinos/squarks at SPS 2	46.03	$9.21 * 10^5$
E	mSUGRA4	191	$3.82 * 10^6$
F	mSUGRA5	203	$4.06 * 10^6$
G	mSUGRA6	600	$1.20 * 10^7$
H	WW	0.84	$1.68 * 10^4$

4 Detector and trigger simulation

The simulation package CMSIM [20] (version 125), which describes the detector geometry and materials, was used to simulate hits in the detector. A hit is described by the location, the magnitude and the time of occurrence of a particle energy deposit in a detector, and CMSIM simulates the effects of energy loss, multiple scattering and showering in the detector materials using the GEANT3 detector simulation tool [21]. The simulation was performed separately for the signal and the pileup minimum bias samples.

The next step was to simulate the response of the detector readout electronics to the deposited energy, mixing signal and pileup and adding electronics noise. The digitized detector hits corresponding to the raw data of a bunch crossing were produced within the Object-oriented Reconstruction for CMS Analysis (ORCA) framework (version 6) [22].

In the electromagnetic calorimeter, the duration of the reconstructed pulse is more than 200 ns. Several neighbouring bunch crossings thus overlap (out-of-time pileup). Therefore the signals of five crossings before and three crossings after the triggered bunch crossing were superimposed. The time of an interaction is by definition that of the maximum of the signal.

The input for the L1 jet trigger are the calorimeter digitizations. The brass/scintillator hadron calorimeter [23] has a nonlinear response, i.e. the average reconstructed energy is smaller than the actual energy deposit due to the non-compensating nature of the brass/scintillator samples. The non-linearity is larger if the energy deposit is smaller. Hadronic showers were simulated using the generator GCALOR [24] with energy cutoffs for photons, electrons, neutral and charged hadrons tuned according to test beam measurements [25]. The nonlinearity is well reproduced in the simulation.

As foreseen in the L1 Calorimeter Trigger hardware implementation, the nonlinearity of the hadronic energy measurement was corrected by correction functions depending on transverse energy and pseudorapidity. The pileup adds energy to the signal, thus alleviating the nonlinearity. This effect is bigger at high luminosity than at low luminosity. The correction function therefore also depends on the luminosity. The high-resolution crystal electromagnetic calorimeter [26] has quite linear a response.

Muons are reconstructed separately in the barrel drift-tube or endcap cathode strip precision chambers and in the RPC trigger chambers. The response of the time-to-digital converters (TDC) forms the output of the digitization step of the barrel drift-tube system. Muon direction and impact position with respect to the sense wire and effects of the residual magnetic field in the air gaps of the magnet iron yoke, where the chambers are located, are taken into account in the simulation [27]. The TDC output signal for the hit reconstruction is obtained from the drift time by adding the muon time-of-flight from the collision vertex and the propagation time of the signal along the cell wire. In case of multiple hits in a cell due to delta rays and/or muon showering, the signal from the hit nearest to the wire is retained.

The digitization step of the cathode strip chamber system involves simulating the response of the analog-to-digital converters and discriminators connected to the strips and wires respectively. A detailed description of the simulation, which includes crosstalk and electronic noise, is given in [28].

The RPC response is assumed to take place within 20 ns of the passage of a charged particle through the detector with a 3 ns Gaussian distributed jitter, which also accounts for the contribution of the front-end electronics and the signal transfer along the cables. The 20-ns-wide time gates were adjusted in order to accommodate triggering signals. The RPC cluster size is set to 1.5 strips, and the average hit efficiency is 95% [29]. The intrinsic chamber noise, to which RPC chambers are most sensitive, is not included in the simulation because of CPU time constraints.

The performance of the Level-1 Trigger system has been simulated in the ORCA framework. It contains a detailed description of the L1 Trigger hardware, mapped into the object-oriented software structure in such a way that each component is represented by an object. Emphasis was put on designing a simulation which closely follows the hardware structure. The simulation models the hierarchy of components from FPGA (field programmable gate arrays) or ASIC (application specific integrated circuits) chip level, through electronics boards, up to the L1 Trigger subsystems. A description of the various hardware components was implemented to mimic exactly the functionality of currently constructed prototypes as described in [1]. Bit-wise arithmetic has been used whenever feasible in the simulation to reproduce the real electronic circuit behaviour as accurately as possible [30].

Table 2. Trigger conditions and thresholds

Trigger conditions	Hardware thresholds [GeV/c or GeV]	95% efficiency thresholds [GeV/c or GeV]
μ	14	14
$\mu\mu$	3	3
e	23	29
ee isolated	12	17
ee all	19	24
τ	93	86
$\tau\tau$	66	59
J	138	180
3 J	66	86
4 J	53	70
J $\not\!\!E_T$	60, 65	88, 120
μ e	4, 13	4, 18
μ τ	4, 55	4, 48
μ J	4, 50	4, 76
μ $\not\!\!E_T$	4, 45	4, 90
$\mu\Sigma E_T$	4, 300	4, 850
e J	15, 100	20, 135
e τ	15, 70	15, 63
$\not\!\!E_T$	140	200
e $\not\!\!E_T$	20, 75	27, 140
ΣE_T	600	1200
H_T	400	470

5 Trigger scenario

In accordance with the capacity of the HLT event filter and the data acquisition (DAQ) at the startup of LHC during the initial low-luminosity running, the maximum output rate of the Level-1 Trigger has been set to 50 kHz. The cross section of the background has been estimated by Monte Carlo studies, and it was assumed that the uncertainty of the result is about a factor two. It was decided to use a safety factor of three, allowing a total Level-1 output rate of approximately 16 kHz dedicated to physics triggers.

A basic trigger menu with the trigger conditions shown in Table 2 has been defined. The thresholds for the trigger objects electrons/photons (denoted as "e"), muons, jets (denoted as "J" and including both central and forward jets), τ jets, missing ($\not\!\!E_T$)and total transverse energies (ΣE_T and H_T) were chosen to yield the permitted total rate of approximately 16 kHz. The muon thresholds and part of the calorimeter thresholds originate from [2]. The remaining calorimeter thresholds are based on scenarios studied in CMS. Both the hardware settings and the values at which the efficiency of the trigger reaches 95% of its maximal value are given. By definition, the two numbers are identical for muons. For τ jets the calibration is derived from ordinary QCD jets, which leads to a systematic overestimation of the τ jet energies at the first trigger level. The allowed bandwidth quota of 16 kHz has been divided into four equal groups among the e/ee, the $\mu/\mu\mu$, the $\tau/\tau\tau$ triggers and the rest, which includes jet triggers, E_T sums and combined triggers. Most of the quota has been assigned to single and double object triggers, since they yield the largest contribution to the signal efficiencies. Multiple (more than two objects) and combined (more than one type of objects) triggers have lower backgrounds and modest contributions to the signal efficiencies.

The trigger menu has neither been optimized for supersymmetry nor for any specific channel. It is a multipurpose menu suitable for any new particle searches, except for heavy ion or b-physics studies, which would require, for example, a lowering of the muon thresholds.

The trigger rates obtained are 3.6 kHz for the muon group, 4.3 kHz for the electron group, 3.0 kHz for the τ group and 3.0 kHz for the pure-jet triggers of the fourth group made of jet and combination triggers. The overall total trigger rate is smaller than the sum of the rates of the four groups because overlaps are possible. The thresholds, meant for an initial LHC luminosity of 2×10^{33} cm^{-2}s^{-1}, will have to be adapted to the actual luminosity conditions during the course of each data taking period. At lower instantaneous luminosities the thresholds could be lowered, which leads to higher Level-1 trigger efficiencies

but generally also to more background in the data sample selected by the Level-1 Trigger. The thresholds for the first three groups and the pure-jet trigger thresholds of the fourth group for the nominal low LHC luminosity are not expected to change significantly in the future. The thresholds for the combined triggers may undergo more retuning, which would affect the individual rate distributions in that group. The additional contribution to the overall rate, however, is small compared to that of the single and double object triggers.

6 Results

The goal of this study was to determine Level-1 trigger efficiencies for selected SUSY events recorded during the initial low-luminosity running period of the LHC. High L1 efficiencies are a prerequisite to large overall efficiencies, which are a convolution of both Level-1 and HLT efficiencies.

The Level-1 trigger efficiency is defined as the ratio of the number of events accepted by the Global Trigger, within the fiducial volume equipped with trigger electronics, and the number of events generated. No geometrical restrictions were applied to the particles in the generation process. Once real data are available, they will be used to determine trigger efficiencies independently of simulated events, with overlapping triggers running in parallel. These can be obtained in several ways. One possibility would be to reduce energy or momentum thresholds, another to relax constraints such as electron or muon isolation requirements. If the trigger rates become too high with the loosened criteria, prescaling of a trigger is possible.

The Level-1 results obtained with the generated samples are summarized in Tables 3 and 4.

The additional and exclusive efficiencies are very important indicators of the usefulness of the particular triggers. The sum of the additional triggers is the overall efficiency of the trigger system for a physics channel. Whilst a particular additional efficiency depends on the order of the triggers, their sum is independent.

The individual, the additional and the exclusive efficiencies of every trigger have been calculated for each channel. The individual efficiency is the efficiency of a trigger as if it were the only trigger applied. In reality several triggers are running in parallel and overlap, i.e., the same event can be selected by more than one trigger. This overlap is excluded by the additional trigger efficiency, which does not count events already found by a previous trigger. The order of triggers as listed in Tables 3 and 4 was used. The exclusive efficiency refers to events found by one and only one trigger, i.e., events found by more than one trigger are not counted here, regardless whether the trigger is previous or subsequent.

The trigger efficiencies for mSUGRA points without specific subprocess constraints are high – 89% to 96% for the mSUGRA channels E, F and G (Table 3). Specific

Table 3. Efficiencies at the global trigger for mSUGRA channels at the upper mass reach of Tevatron Run II

Trigger	Hardware thresholds	ε_E(mSUGRA4) [%]			ε_F(mSUGRA5) [%]			ε_G(mSUGRA6) [%]		
	[GeV/c or GeV]	ind.	add.	exc.	ind.	add.	exc.	ind.	add.	exc.
μ	14	18.5	18.5	0.5	18.9	18.9	0.1	17.2	17.2	0.5
$\mu\mu$	3	7.4	1.6	0	6.9	1.1	0	5.0	0.9	0
e	23	12.0	10.2	0.3	12.5	10.3	0.1	10.6	9.2	0.2
ee isol.	12	2.9	1.1	0.1	4.5	0.9	0	4.6	1.7	0
ee all	19	4.5	3.3	0	4.4	3.0	0	5.9	4.9	0.2
J	138	82.8	53.8	0.6	86.8	56.8	0.1	70.1	44.7	0.1
3 J	66	55.9	2.5	0.3	61.5	1.7	0.1	63.8	6.1	0.3
4 J	53	38.3	0.3	0	46.1	0.4	0	54.9	1.3	0.2
J $\not\!\!E_T$	60, 65	85.3	3.5	1.7	84.2	2.6	0.7	64.6	1.9	0.8
τ	93	46.6	0.6	0.4	49.8	0.4	0.3	46.2	0.5	0.4
$\tau\tau$	66	26.7	0.2	0.1	29.0	0	0	34.0	0.2	0.1
μ e	4, 13	6.2	0.1	0.1	6.6	0	0	7.6	0.1	0
μ τ	4. 55	21.7	0.2	0	22.0	0	0	24.3	0.1	0
μ J	4, 50	29.5	0.3	0	29.1	0.2	0.1	29.1	0.1	0.1
μ $\not\!\!E_T$	4, 45	27.5	0	0	27.1	0	0	24.3	0	0
$\mu\Sigma E_T$	4, 300	21.6	0	0	25.0	0	0	22.7	0	0
e J	15, 100	18.4	0	0	18.0	0	0	17.7	0	0
e τ	15, 70	14.5	0	0	14.7	0	0	14.9	0	0
$\not\!\!E_T$	140	54.9	0	0	53.3	0	0	24.5	0	0
e $\not\!\!E_T$	20, 75	12.4	0	0	10.6	0	0	7.9	0	0
ΣE_T	600	29.1	0	0	33.1	0	0	22.4	0	0
H_T	400	50.6	0	0	57.1	0	0	43.0	0	0
Total Efficiency		96.2 ± 3.0 (stat.)			96.3 ± 3.0 (stat.)			88.9 ± 2.8 (stat.)		

Table 4. Efficiencies at the Global Trigger for smuons, charginos and neutralinos, gluinos and squarks, and W^+W^-

Trigger	Hardware thresholds	$\varepsilon_A(\tilde{\mu}_L\tilde{\mu}_L)$ [%]			$\varepsilon_B(\tilde{\chi}_2^0\tilde{\chi}_1^\pm)$ [%]			$\varepsilon_C(\tilde{g}/\tilde{q})_{SPS1a}$ [%]			$\varepsilon_D(\tilde{g}/\tilde{q})_{SPS2}$ [%]			$\varepsilon_H(WW)$ [%]		
	[GeV/c or GeV]	ind.	add.	exc.	ind.	add.	exc.	ind.	add.	exc.	ind.	add.	exc.	ind.	add.	exc.
μ	14	92.5	92.5	16.7	49.0	49.0	12.3	27.8	27.8	0	40.8	40.8	0	80.5	80.5	33.5
$\mu\mu$	3	68.8	0.1	0.0	24.6	2.9	1.8	13.8	1.3	0	24.3	3.6	0	43.4	0.1	0.1
e	23	3.3	0.3	0.3	22.9	13.1	4.2	19.7	14.9	0	20.2	11.7	0	0.9	0.2	0.1
ee isol.	12	0.5	0	0	8.9	1.9	1.2	8.6	0.5	0	7.1	0.6	0	0.1	0	0
ee all	19	0	0	0	0	0	0	5.9	3.5	0	10.0	5.3	0	0	0	0
J	138	3.7	0.2	0	1.4	0.2	0	88.4	47.0	0.1	98.7	37.7	0	0.2	0.1	0
3 J	66	0.1	0	0	0.2	0	0	68.6	1.5	0.1	97.6	0.3	0	0	0	0
4 J	53	0.1	0	0	0.1	0	0	53.1	0.3	0.2	94.8	0	0	0	0	0
J $\not\!\!E_T$	60, 65	7.8	0.3	0.2	5.3	0.8	0.4	84.8	0.8	0.4	92.2	0	0	0.6	0.1	0.1
τ	93	4.9	0	0	4.4	0.2	0.1	55.2	0.1	0	68.2	0	0	0.5	0	0
$\tau\tau$	66	0.6	0	0	0.9	0	0	33.2	0.1	0	51.0	0	0	0.1	0	0
μ e	4, 13	5.0	0	0	26.0	2.7	2.3	11.1	0	0	19.3	0	0	2.2	0.1	0.1
μ τ	4, 55	14.3	0	0	14.2	0.4	0	31.6	0	0	53.2	0	0	2.6	0.2	0
μ J	4, 50	25.1	0	0	22.7	0.9	0.7	38.6	0.1	0	59.1	0.1	0	6.5	0.1	0.1
μ $\not\!\!E_T$	4, 45	13.6	0	0	9.3	0.1	0.1	35.1	0	0	56.9	0	0	2.0	0.1	0.1
$\mu\Sigma E_T$	4, 300	2.2	0	0	1.3	0	0	34.1	0	0	58.8	0	0	1.2	0	0
e J	15, 100	1.2	0	0	3.7	0	0	26.5	0	0	28.4	0	0	0.1	0	0
e τ	15, 70	1.4	0	0	8.4	0.1	0.1	23.2	0	0	24.9	0	0	0.4	0	0
$\not\!\!E_T$	140	1.7	0	0	0.3	0	0	61.1	0	0	67.5	0	0	0.1	0	0
e $\not\!\!E_T$	20, 75	1.2	0	0	2.1	0	0	18.5	0	0	20.1	0	0	0.2	0	0
ΣE_T	600	0.1	0	0	0	0	0	39.3	0	0	86.2	0	0	0.1	0	0
H_T	400	0.1	0	0	0	0	0	64.5	0	0	96.3	0	0	0	0	0
Total Efficiency		93.4 ± 3.0 (stat.)			72.3 ± 2.3 (stat.)			97.9 ± 3.1 (stat.)			100.0 ± 3.2 (stat.)			81.3 ± 1.8 (stat.)		

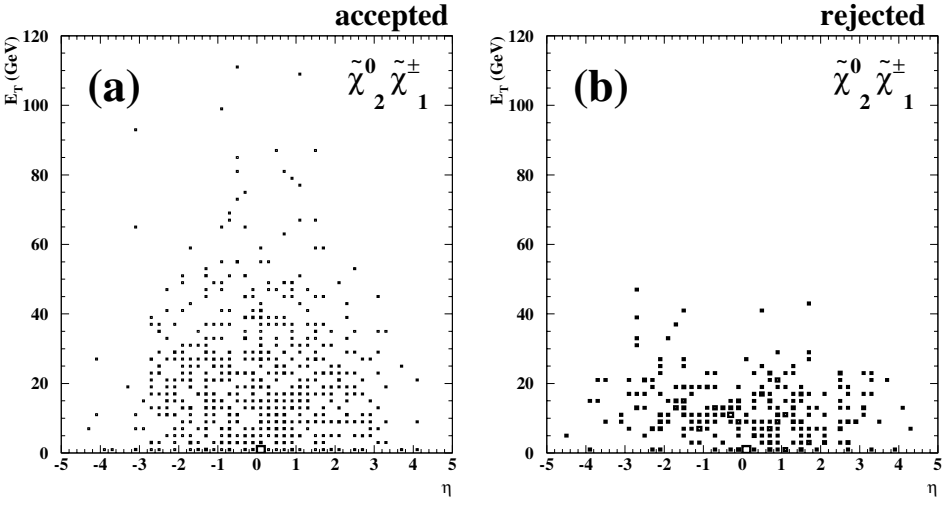

Fig. 4. The E_T vs. η distribution of the generated (PYTHIA) highest-energy electrons in $\tilde{\chi}_2^0\tilde{\chi}_1^\pm$ events accepted **a** and rejected **b** by the L1 Trigger

final states show a larger spread in efficiencies (Table 4 for channels A to D and H), ranging from 72% to 100%.

Channel B has the lowest efficiency. It has three charged leptons (electrons or muons), two neutralinos and seven neutrinos in the final state, coming from the decay of the $\tilde{\chi}_2^0\tilde{\chi}_1^\pm$ pair. Despite the good electron and muon detection efficiencies, only about 70% of the Channel B events are selected, even though the leptons are produced from two initial charginos and neutralinos of around 200 GeV/c^2. In the events rejected by the trigger, in many cases either the electrons have very low E_T (Figs. 4 and 5) or the pseudorapidities of the muons are beyond the $|\eta| < 2.1$ coverage of the muon trigger (Figs. 6 and 7).

It was investigated whether a substantial fraction of the energy is carried by invisible particles and whether a trigger on missing transverse energy could be used as a consequence. A dielectron-plus-missing-E_T trigger with symmetric thresholds of 8 GeV for the two electrons and 20 GeV for $\not\!\!E_T$ respectively was used. The scalar energy sum and the scalar and vector transverse energy sums of the invisible particles mentioned above were checked. It was found that the energy sum was larger for the rejected

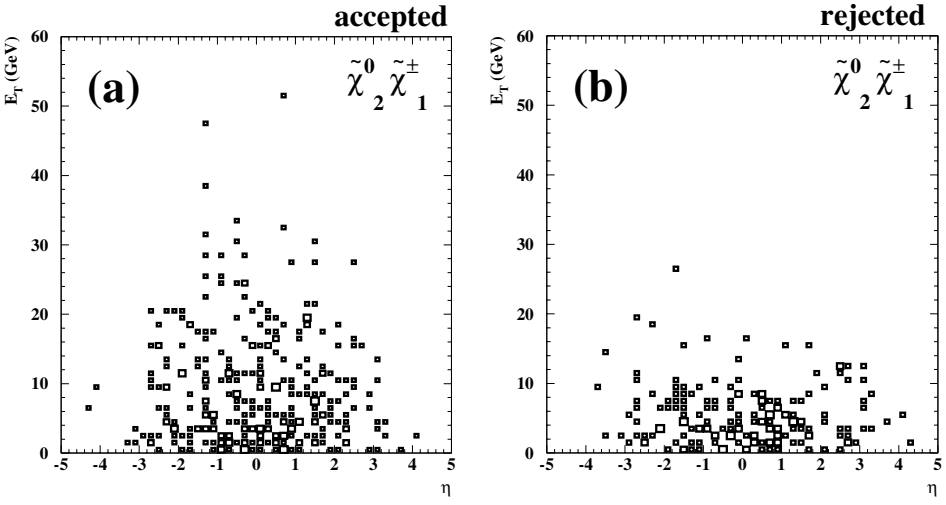

Fig. 5. The E_T vs. η distribution of the generated (PYTHIA) second-highest-energy electrons in $\tilde{\chi}^0_2\tilde{\chi}^\pm_1$ events accepted **a** and rejected **b** by the L1 Trigger.

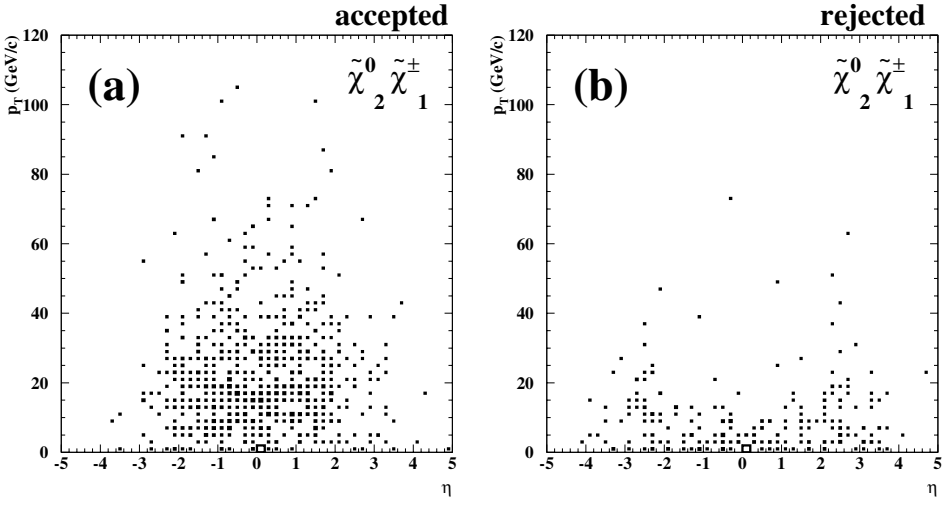

Fig. 6. The p_T vs. η distribution of the generated (PYTHIA) highest-momentum muons in $\tilde{\chi}^0_2\tilde{\chi}^\pm_1$ events accepted **a** and rejected **b** by the L1 Trigger

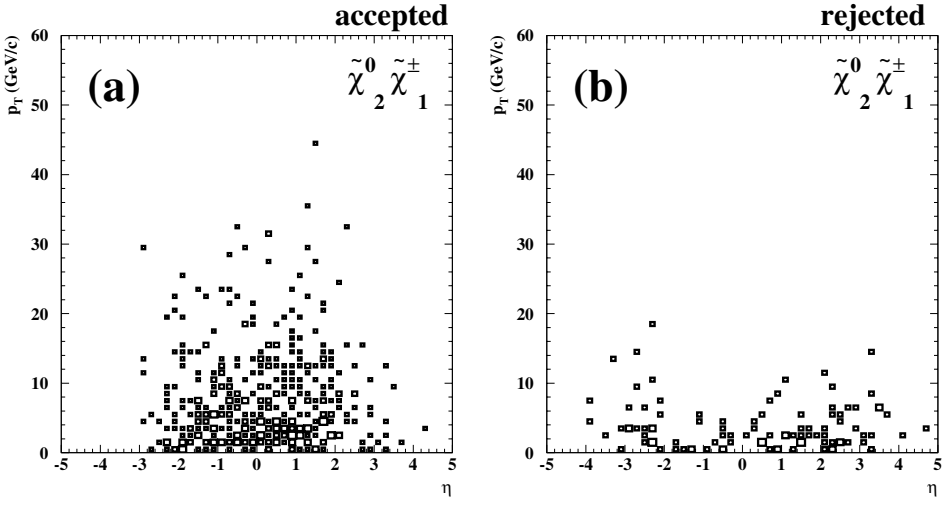

Fig. 7. The p_T vs. η distribution of the generated (PYTHIA) second-highest-momentum muons in $\tilde{\chi}^0_2\tilde{\chi}^\pm_1$ events accepted **a** and rejected **b** by the L1 Trigger

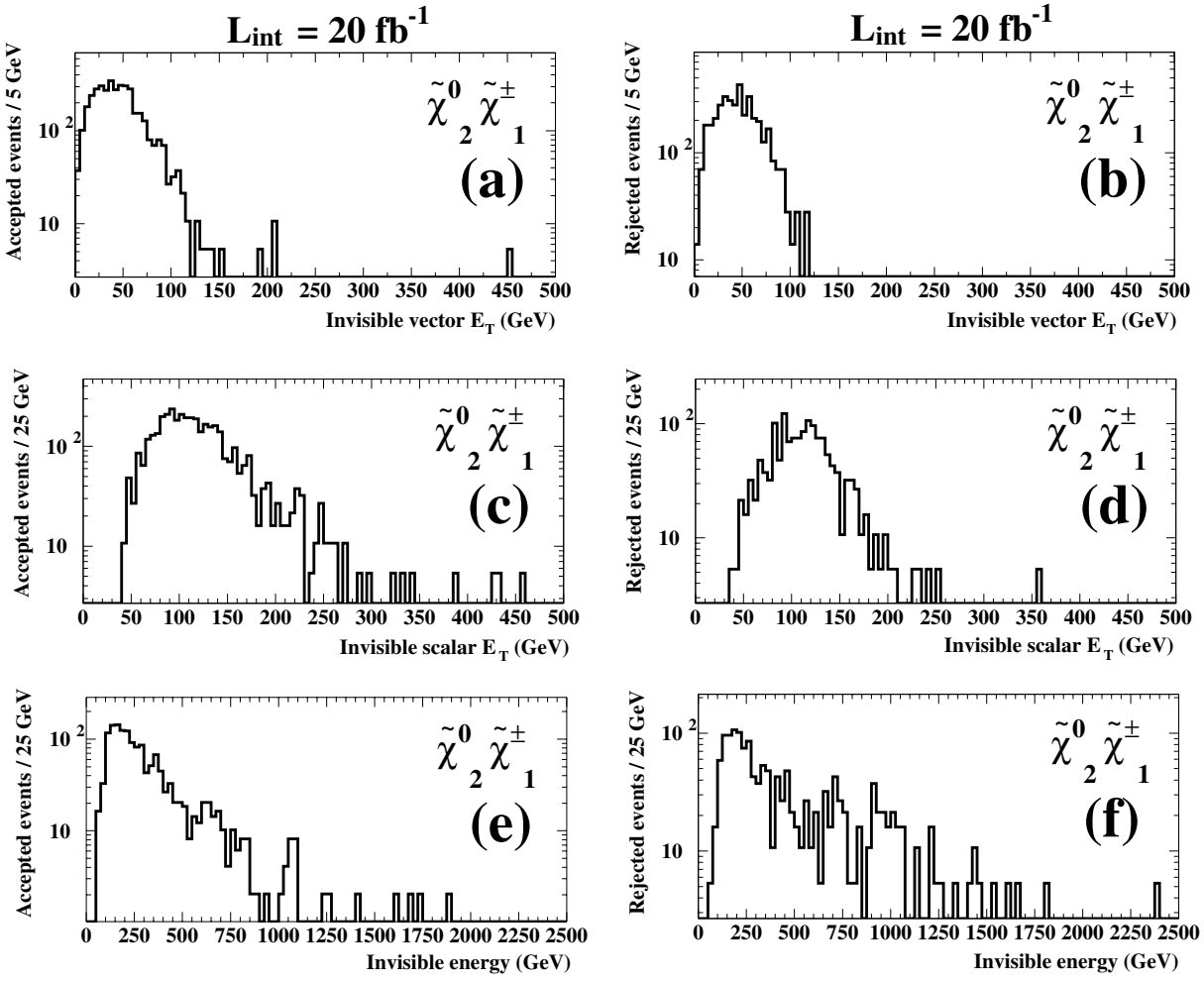

Fig. 8. The generated vector E_T sums *(a), (b),* scalar E_T sums *(c), (d),* and the scalar energy sums *(e), (f)* of invisible particles of the $\tilde{\chi}_2^0\tilde{\chi}_1^\pm$ events accepted *(a), (c), (e)* and rejected *(b), (d), (f)* by the L1 Trigger

events than for those passing the trigger, while the scalar and vector E_T sums were approximately the same (Fig. 8). This can arise because particles may be produced at higher rapidites due to a larger longitudinal boost for the original SUSY particles or because the invisible particles in the rejected events balance their (large) E_T contributions. With many weakly interacting particles in the event, the probability of such a cancellation is enhanced. However, the dielectron-plus-missing-E_T trigger would only marginally increase the efficiency.

The trigger efficiencies listed in Tables 3 and 4 are functions of the thresholds, of the energy or momentum resolution and geometrical acceptance of the L1 Trigger. To give a qualitative evaluation of the different effects, two channels (A and C) were specifically investigated with respect to the muon trigger. The smuon channel A has a high muon trigger efficiency – about 93% for the single muon trigger and 69% for the dimuon trigger respectively. The corresponding numbers for the gluino/squark channel C decaying predominantly into leptons are only about 28% and 14%.

Figure 9 shows the transverse momentum spectra of the two highest-p_T muons tracked through the detector for the smuon channel A and for the gluino/squark channel C. The corresponding transverse momenta and pseudorapidities of the two highest-p_T muon candidates at the output of the L1 Global Muon Trigger are shown in Figs. 10 and 11, respectively. The dashed lines indicate the p_T threshold of 14 GeV/c for the single muon trigger in Fig. 10 and the η coverage limits of the muon trigger in Fig. 11. In the L1 Muon Trigger a nonlinear p_T scale with 32 p_T intervals is used. The intervals are smaller at lower than at higher p_T values. All muon candidates with transverse momenta higher than 140 GeV/c are assigned to the 140 GeV/c bin.

The high single muon trigger efficiency for the smuon channel A is due to the high momenta of the original muons. For the gluino/squark channel C, with fewer muons than channel A, many muons do not pass the threshold of 14 GeV/c. In both channels, losses due to

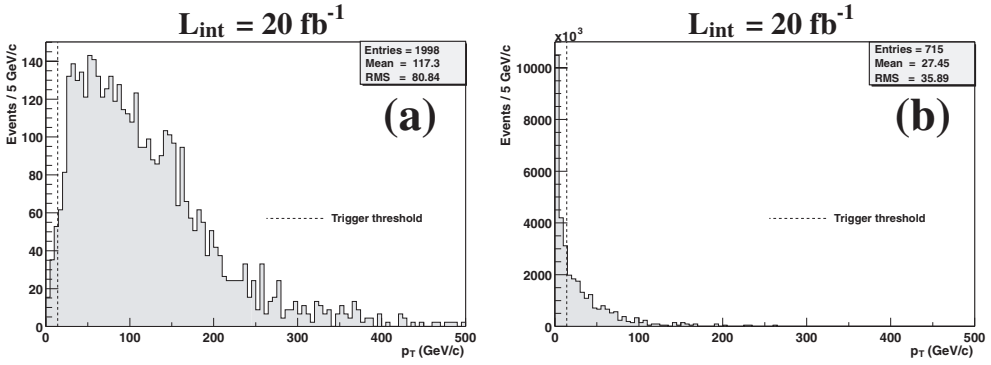

Fig. 9. The p_T distributions of the two highest-p_T muons in the smuon channel A **a** and the gluino/squark channel C **b**

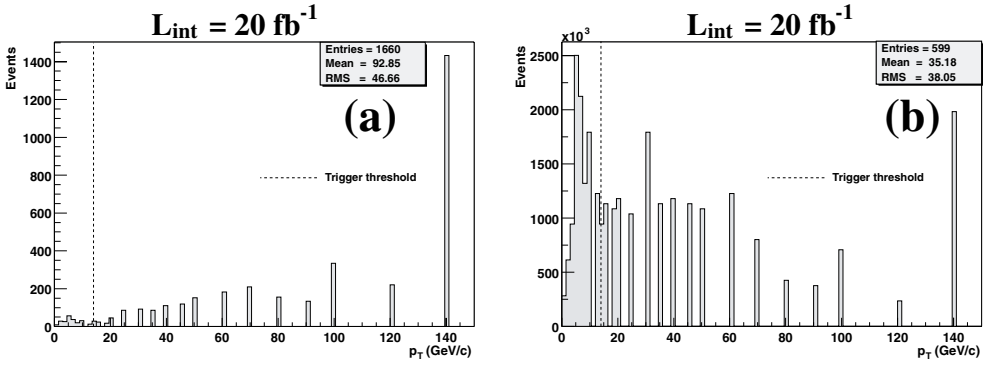

Fig. 10. The p_T distributions of the two highest-p_T L1 muon candidates for the smuon channel A **a** and the gluino/squark channel C **b**

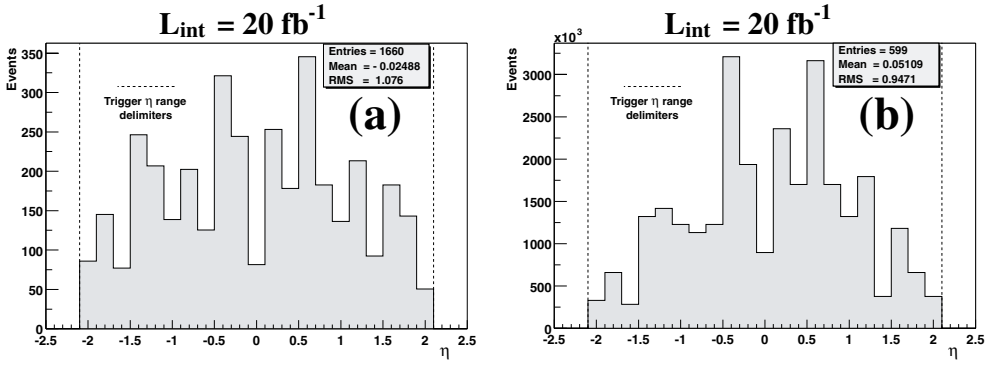

Fig. 11. The η distributions of the two highest-p_T L1 muon candidates for the smuon channel A **a** and the gluino/squark channel C **b**

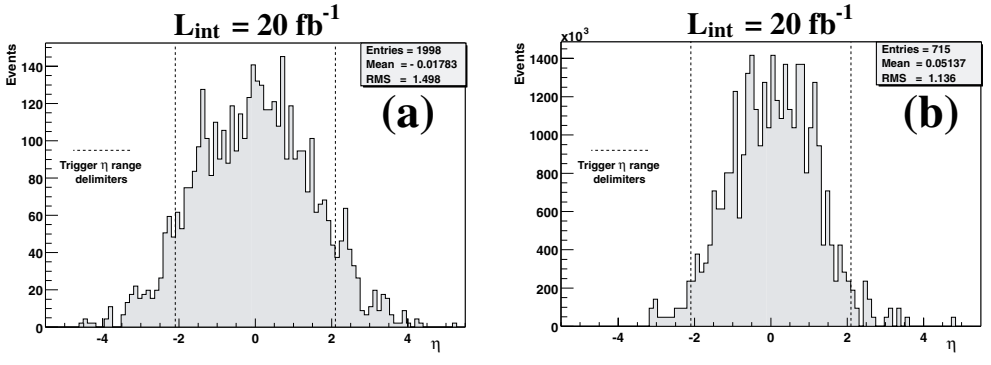

Fig. 12. The η distributions of the two highest-p_T muons for the smuon channel A **a** and the gluino/squark channel C **b**

the limited η coverage of the muon trigger play a less important role, as can be seen from Fig. 12, which shows the pseudorapidity distributions of the two highest-p_T muons for channels A and C, respectively.

To evaluate the physics potential of CMS the convoluted Level-1 and High-Level Trigger efficiencies have to be calculated. Combined L1 and HLT efficiencies for some supersymmetry scenarios have been estimated in [2]. The actual values depend very much on the trigger parameters chosen. For example, mSUGRA4 triggered by the jet-plus-missing-energy algorithm with L1 95% efficiency thresholds of 79 GeV and 46 GeV respectively, is selected with an L1 efficiency of 88%. The combined L1/HLT efficiency for HLT cuts of 180 GeV for the jet and 123 GeV for the missing energy is 67%. The mSUGRA6 channel efficiency is 71% at L1, whilst it is only 37% after HLT for the same cuts. If, at Level-1, a three-jet trigger with a 95% efficiency threshold of 86 GeV for each jet and, at the High-Level Trigger, a four-jet trigger with thresholds of 113 GeV are used in addition, the mSUGRA4 efficiency decreases from 92% at L1 to 69% after HLT, and the mSUGRA6 efficiency from 85% to 44%. These efficiencies can be improved by adding more algorithms and optimizing the conditions for supersymmetry once LHC is turned on.

7 Conclusions

The efficiencies to trigger on supersymmetric events with the CMS Level-1 Trigger have been studied. Calculations have been performed for the production of smuon pairs, charginos/neutralinos, gluinos/squarks and events generated at selected strategic points in the mSUGRA parameter space. A WW control channel with the W's decaying into $\mu\nu_\mu$ was also studied. The energy and momentum thresholds were chosen to yield a total Level-1 trigger rate of about 16 kHz at a luminosity of 2×10^{33} cm^{-2}s^{-1}, allowing for a safety factor three with respect to the maximum High-Level Trigger input rate of 50 kHz.

The Level-1 efficiencies are high in the majority of the studied channels, between 89% and 96% for the general mSUGRA channels, between 93% and 100% for the smuon and gluino/squark channels and 81% for the WW channel. The chargino/neutralino channel shows the lowest efficiency, about 72%. This arises due to particles being produced at higher rapidities, but in part also due to the fact that a large fraction of the energy is carried away by invisible particles and that the net missing transverse energy of the events may be balanced.

The final efficiencies to trigger on interesting events depend both on the Level-1 and the High-Level Trigger. The HLT in particular has a large potential to optimize its conditions for the on-line selection of supersymmetric events.

Acknowledgements. We would like to thank the Austrian Exchange Service (Österreichischer Austauschdienst) and the Hungarian government for their financial support (contract numbers A-28/2000 and TéT A-28/2000 respectively). We are grateful for a substantial grant by the City of Vienna's Jubilee Fund for the Austrian Academy of Sciences (Jubiläumsfonds der Stadt Wien für die Österreichische Akademie der Wissenschaften) and acknowledge support by INTAS (project reference INTAS-CERN 99 nr. 558). We are indebted to our CMS colleagues S. Abdullin, S. Arcelli, P. Chumney and A. Nikitenko for their help. We also thank the numerous physicists, engineers and technicians that have made contributions to simulation software, analysis tools and Monte Carlo productions as well as detector and trigger development. D. Acosta, P. Janot, and D. Newbold are thanked for internal refereeing of this paper.

References

1. The TriDAS Project – The Level-1 Trigger Technical Design Report, CERN/LHCC 2000-38 (2000)
2. The TriDAS Project – Data Acquisition and High-Level Trigger Technical Design Report, CERN/LHCC 2002-26 (2002)
3. J. Lackey et al., CMS Note 1998/074 (1998)
4. G.P. Heath, Nucl. Instr. Meth. A **461** (2001) 505
5. F. Gasparini et al., Nucl. Instr. Meth. A **336** (1993) 91
6. J. Hauser, Proceedings of the Fifth Workshop on Electronics for LHC Experiments, Snowmass, Co., USA, Sept. 1999, CERN/99-09, CERN/LHCC/99-33 (1999) 304
7. J. Erö, Proceedings of the Fifth Workshop on Electronics for LHC Experiments, Snowmass, Co., USA, Sept. 1999, CERN/99-09, CERN/LHCC/99-33 (1999) 309
8. D. Acosta et al., Nucl. Instr. Meth. A **496** (2003) 64; D. Acosta et al., Proceedings of the Seventh Workshop on Electronics for LHC Experiments, Stockholm, Sweden, Sept. 2001, CERN/2001-005, CERN/LHCC/2001-034 (2001) 243; D. Acosta et al., Proceedings of the Fifth Workshop on Electronics for LHC Experiments, Snowmass, Co., USA, Sept. 1999, CERN/99-09, CERN/LHCC/99-33 (1999) 318
9. M. Andlinger et al., Nucl. Instr. Meth. A **370** (1996) 389
10. H. Sakulin, M. Fierro, CMS Note 2001/003 (2001)
11. C.-.E. Wulz, Nucl. Instr. Meth. A **473** (2001) 231; A. Taurok, H. Bergauer, M. Padrta, Nucl. Instr. Meth. A **473** (2001) 243
12. B.C. Allanach et al., Eur. Phys. J. C **25** (2002) 113
13. N. Ghodbane, H.-U. Martyn, hep-ph/0201233 (2002)
14. S. Abel et al., hep-ph/0003154 (2000)
15. H. Baer et al., Phys. Rev. D **51** (1995) 1046; H. Baer et al., Phys. Rev. D **52** (1995) 2746
16. T. Sjöstrand et al., Comput. Phys. Commun. **135** (2001) 238
17. S. Mrenna, Comput. Phys. Commun. **101** (1997) 232
18. H. Baer, F.E. Paige, S.D. Protopopescu, X. Tata, hep-ph/0001086 (2000). Version 7.51 was used for this study.
19. H. Lai et al., Eur. Phys. J. C **12** (2000) 375
20. http://cmsdoc.cern.ch/cmsim/cmsim.html; C. Charlot et al., C MS TN/93-63 (1993)
21. GEANT3 Detector Description and Simulation Tool, CERN program library long writeup W5013, release 15111999 (1999)
22. CMS Object Oriented Reconstruction, http://cmsdoc.cern.ch/orca/
23. The CMS Hadron Calorimeter Project – Technical Design Report, CERN/LHCC 97-31 (1997)

24. C. Zeitnitz, T. A. Gabriel, Nucl. Instr. Meth. A **349** (1994) 106; http://wswww.physik.uni-mainz.de/zeitnitz/gcalor/gcalor_manual.ps
25. V. V. Abramov et al., Nucl. Instr. Meth. A **457** (2001) 75
26. The CMS Electromagnetic Calorimeter Project – Technical Design Report, CERN/LHCC 97-33 (1997)
27. A. Gresele, T. Rovelli, CMS Note 1999/064 (1999)
28. R. Wilkinson, P. T. Cox, CMS Note 2001/013 (2001)
29. G. Bruno, M. Konecki, CMS Note 2001/012 (2001)
30. D. Acosta, M. Stoutimore, S.M. Wang, CMS Note 2001/033 (2001)